JOURNAL OF GEOPHYSICAL RESEARCH, VOL. 112, D03203, doi:10.1029/2006JD007267, 2007

Estimation of aerosol optical properties and radiative effects in the Ganga basin, northern India, during the wintertime

Sagnik Dey[1] and S. N. Tripathi[1]

Received 7 March 2006; revised 13 September 2006; accepted 2 October 2006; published 7 February 2007.

[1] An aerosol model has been developed using mass size distributions of various chemical components measured at Kanpur (an urban location in the Ganga basin, GB, in northern India) and applied to estimate the radiative effects of the aerosols over the entire GB during the winter season. The number size distribution of various species was derived from the measured mass concentration, and the optical properties were calculated using Mie theory. The maximum anthropogenic contribution to the total extinction was estimated to be ~83%. The relative contributions of various species to the aerosol optical depth (AOD) at 0.5 μm are in the following order: $(NH_4)_2SO_4$ (nss-SO_4, 30%), nitrate (NO_3^-, 24%), salt (mainly NaCl and KCl, 18%), dust (17%) and black carbon (BC, 11%). Relative contribution of nss-SO_4, NO_3^- and salt to the calculated AOD decreases with wavelength, and that of dust increases with wavelength, whereas BC contribution is spectrally insensitive. The extinction coefficient strongly depends on the RH, as the scattering by fine mode fraction, which contributes 88% to the total extinction, is enhanced at high ambient RH. The spectral variation of absorption coefficient indicates that the most likely source of BC in this region is fossil fuel. The spectral variation of single scattering albedo (SSA) in the coarse mode fraction suggests mixing of BC and dust particles. During the observational period, the mean shortwave (SW) clear sky top of the atmosphere (TOA) and surface forcing over Kanpur are estimated to be -13 ± 3 and -43 ± 8 W m^{-2}, respectively. The corresponding longwave forcings are 3.6 ± 0.7 and 2.9 ± 0.6 W m^{-2}, respectively. Mean AOD at 0.55 μm over the GB as derived from MODIS data is 0.36 ± 0.14. Extending our model over the entire GB, the net mean TOA and surface forcing become -6.4 and -30.2 W m^{-2} (with overall ~15% uncertainty). This results in high atmospheric absorption (+23.8 W m^{-2}), translating into a heating rate of 0.67 K day^{-1}. The SW surface to TOA forcing ratio (~3.7) over the GB is 23% higher than the corresponding value for Indian Ocean. The aerosols reduce the incoming solar radiation reaching the surface by ~19%, which has significant effect on the regional climate.

Citation: Dey, S., and S. N. Tripathi (2007), Estimation of aerosol optical properties and radiative effects in the Ganga basin, northern India, during the wintertime, *J. Geophys. Res.*, *112*, D03203, doi:10.1029/2006JD007267.

1. Introduction

[2] It is now a well-known fact that the aerosols perturb the Earth-atmosphere radiation budget by attenuating the solar radiation. However, uncertainty in estimation of aerosol radiative forcing still persists not only in global scale, but in regional scale also [*Houghton et al.*, 2001], because of lack of knowledge of aerosol optical, microphysical and chemical properties simultaneously, as these are highly variable in spatiotemporal domain. Ever since the Indian Ocean Experiment (INDOEX) was conducted [*Ramanathan et al.*, 2001], which has shown that enormous pollution transported from the Indian subcontinent to the adjacent oceanic regions affected the regional forcing significantly, the focus to characterize the aerosols over Indian landmass and adjacent oceans has intensified. Sensing the need for observational data in order to estimate the radiative forcing more accurately, after the INDOEX, several campaigns have been conducted over the Arabian Sea, Bay of Bengal and tropical Indian Ocean in different seasons [*Satheesh*, 2002a; *Satheesh et al.*, 2006; *Moorthy et al.*, 2003, 2005a; *Sumanth et al.*, 2004; *Vinoj et al.*, 2004; *Ganguly et al.*, 2005a; *Ramachandran*, 2005a, 2005b]. The measured aerosol physical properties in these oceanic regions have been used to derive the optical properties, which subsequently have been used to estimate the aerosol radiative forcing [*Satheesh et al.*, 1999, 2002; *Ramachandran*, 2005a, 2005b; *Moorthy et al.*, 2005a].

[3] Considering the variability of the pollution sources over the Indian landmass, observational data are scanty and isolated. Moreover, simultaneous measurements of physical,

[1]Department of Civil Engineering, Indian Institute of Technology, Kanpur, India.

0148-0227/07/2006JD007267$09.00

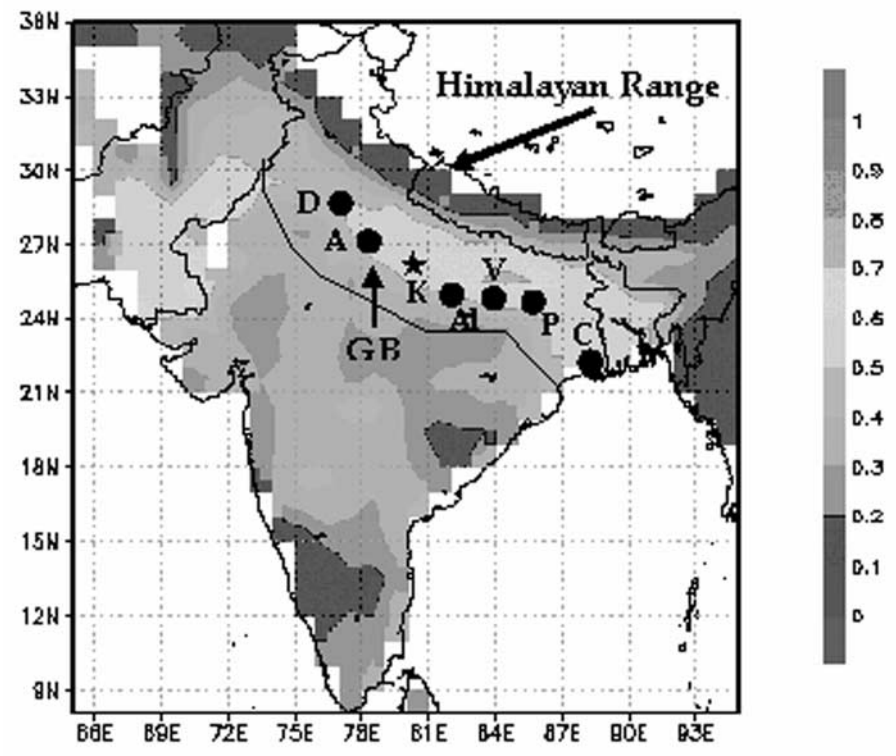

Figure 1. Composite AOD at 0.55 μm wavelength over India as observed by Moderate Imaging Spectroradiometer on board Terra satellite during the campaign period. The locations of Kanpur (K) and the other major cities in the GB Delhi (D), Agra (A), Allahabad (Al), Varanasi (V), Patna (P), and Kolkata (C) are marked. The salient feature is an aerosol pool ($AOD_{0.55} > 0.5$ indicated by lighter shading) existing over the entire central Ganga basin (GB) stretching from Delhi to Kolkata.

optical and chemical properties, which together are essential in understanding the role of aerosols in climate change, are practically nonexistent. Very few studies on the measurements of aerosol parameters and estimation of radiative forcing over the Indian subcontinent exist in the literature [*Moorthy et al.*, 2005b; *Ramanathan and Ramana*, 2005; *Pandithurai et al.*, 2004; *Babu and Moorthy*, 2002; *Babu et al.*, 2002]. *Reddy and Venkataraman* [2000] used fuel consumption data of 1990 in regional scale to build a $PM_{2.5}$ emission inventory and subsequently using a box model, predicted the optical and radiative effects of the anthropogenic aerosols over India. However, their analysis was restricted for the fine mode fraction only. Their estimates were based on the average of whole India; for example, maximum AOD calculated was 0.19, which is far less than the values observed in the Ganga basin (GB, 22–32°N, 74–90°E). Nonetheless, their results showed the need for development of more region-specific models, which can be used to minimize the uncertainty in the global models.

[4] In this context, land campaigns were initiated by Indian Space Research Organization Geosphere Biosphere Program (ISRO-GBP) in the southern India [*Moorthy et al.*, 2005b] during the winter season (February–March) of 2004. During December 2004 to January 2005, the campaign was conducted in the northern India with special attention to the GB. Detailed measurements of several aerosol parameters and size-segregated chemical composition of aerosols were performed in seven major locations in the GB. Kanpur (Figure 1) is one location, where simultaneously optical, physical and chemical measurements were conducted. The observational data were then used to estimate aerosol optical and radiative properties, which could be representative of the GB for the winter season, when the pollutants are being transported from the Indian mainland to the adjacent oceanic regions.

[5] In this paper, we report the salient features of our model, which assesses the relative contribution of different species to the scattering and absorption of solar radiation. The effect of humidity on the observed optical properties is also investigated. Finally, the radiative forcing was estimated and its implications and applicability to the GB are discussed. Earlier, comparative study between MODIS and AERONET-derived aerosol optical depth (AOD) over Kanpur by *Tripathi et al.* [2005a] indicated the need to modify the existing algorithm of MODIS during the dust-loading periods. Similarly, this study along with the AERONET measurements will provide better estimate of the anthropogenic influence of the aerosols in the GB.

2. Background

[6] GB, with more than 500 million population, is one of the most polluted regions in the world, where strong urban

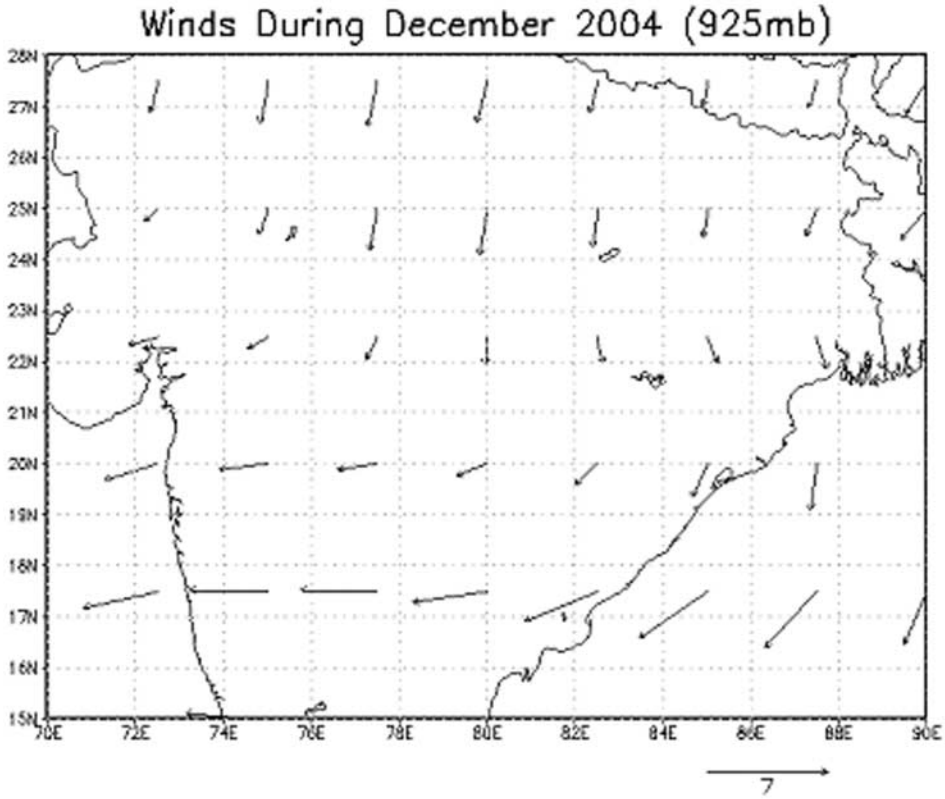

Figure 2. Regional wind vector at 925 hPa during December 2004 to January 2005 as derived from NCEP data.

haze contributes to regional atmospheric brown clouds [*Ramanathan and Ramana*, 2005]. The locations of the measurement site (Kanpur) and other major cities in GB are shown in Figure 1 on a background map of AOD at 0.55 μm derived from MODIS data averaged for December 2004 to January 2005. It is clear from the satellite data that during this time of the year, an elevated aerosol layer (AOD > 0.5) persists over the entire GB. Recently, several studies have reported high AOD over the GB during the winter season as observed from both satellite data [*Girolamo et al.*, 2004; *Jethva et al.*, 2005] and ground-based measurements [*Dey et al.*, 2004, 2005; *Singh et al.*, 2004]. However, the relative contribution of scattering and absorbing species to the observed optical depth, the state of mixing of different components, the nature of hygroscopic growth of the particles, the radiative forcing efficiency are still not known in detail because of lack of collocated data of physical, chemical and optical properties.

[7] So far, information on aerosol chemical composition and size distribution in GB is only available for Delhi (28.67°N, 77.21°E), Agra (27.19°N, 78.01°E) and Kanpur (26.47°N and 80.33°E) during the wintertime. In Agra, size-segregated aerosol chemical composition was analyzed during the monsoon (July–September) season [*Parmar et al.*, 2001], whereas during the winter, only size distribution is available [*Chate and Pranesha*, 2004]. Even in Delhi, only particle number concentration is measured. The meteorological conditions during the monsoon and winter season are quite different in the GB, so the aerosol speciation in the monsoon season cannot be a representative of the wintertime. Hence we have used the chemical composition data of Kanpur measured during ISRO-GBP land campaign II as the basic input of our model.

[8] The sampling location in Kanpur was Indian Institute of Technology Kanpur (IITK) campus, which is ~16 km away from the city center in the upwind side. The regional wind as derived from NCEP data is mainly northerly (Figure 2), however the local surface wind varied from northwesterly to southwesterly [*Tripathi et al.*, 2006]. Very low wind speed (calm condition in ~48% time) along with shallow boundary layer height (as inferred from balloonsonde data [*Tripathi et al.*, 2005b]) lead to poor dispersal of the boundary layer aerosols. Although, the winter season in the Indian subcontinent is termed as "dry winter," because of the western disturbances leading to strong haze and fog mainly in the GB, the relative humidity (RH) soars above 75% during the nighttime and the early morning. During the hazy and foggy days, RH remains high (>60%) throughout the day. However, in the clear days, RH dips down to 40% during the noontime. Hence RH plays an important role in changing the optical properties of aerosol through growth of the hygroscopic components. During the campaign, black carbon (BC) concentration was measured using an Aethalometer (model AE-18, Magee Scientific Inc., USA) both at the surface [*Tripathi et al.*, 2005c] and in the vertical column [*Tripathi et al.*, 2005b]. BC mass fraction, F_{BC} (~10%) was higher during December 2004 than that observed during INDOEX [*Satheesh et al.*, 1999] and

Table 1. Aerosol Mass in the Fine and Coarse Mode Fractions During the Observation Period[a]

Species	Minimum	Maximum	Mean
BC	5.3	20.9	12 ± 5.4
nss-SO_4	21.4, 5.48	53.6, 15.22	34.04 ± 11.55, 8.84 ± 3.89
NO_3^-	14.95, 2.84	44.27, 10.2	26.82 ± 10.17, 5.93 ± 2.28
Salt	6.61, 0.9	14.4, 2.73	11.24 ± 2.43, 1.68 ± 0.6
Dust	0.7, 2.25	2.07, 8.125	1.09 ± 0.44, 5.46 ± 1.7

[a]Unit is $\mu g\ m^{-3}$. The first value is for fine mode fraction, and the second value is for the coarse mode fraction.

corresponds to TOA and surface forcing of +9 ± 3 and −62 ± 23 W m^{-2} [*Tripathi et al.*, 2005c]. However, the net radiative forcing for the composite aerosol can be obtained from the detailed chemical measurements, which are presented in the following sections.

3. Experimental Setup and Methodology

3.1. Measurements and Data

[9] Extensive measurements of aerosol parameters (physical, chemical and optical) were carried out on a roof top in IITK campus during December 2004 to January 2005 as part of ISRO-GBP land campaign II. Aerosol optical properties were measured by CIMEL Sun photometer deployed in IITK under AERONET program, whereas composite aerosol mass and number size distributions were measured using a quartz-crystal microbalance and optical particle counter, respectively (for more detailed description of the objectives and protocol of the measurements, visit http://www.isro.org/gbp/campaign.htm). For chemical characterization, aerosol samples were collected using a four-stage (the size ranges: particle diameter, $D_P < 0.49\ \mu m$, $0.49 < D_P < 0.95\ \mu m$, $0.95 < D_P < 3\ \mu m$ and $3 < D_P < 10\ \mu m$ in the four stages, respectively) Cascade impactor (Pacwill Tisch Environmental, USA) sampler, at a flow rate of 1.13 $m^3\ min^{-1}$. Quartz substrates (Tisch Environmental, USA) were used in all stages except in 1st stage, in which Whatmann GF/A filter papers of size 8″ * 10″ were used. The water-soluble and acid-soluble ion concentrations in fine (first two stages) and coarse (last two stages) were measured by Metrohm 761 Compact Ionic Chromatograph (IC) and Varian SpectrAA 220FS Atomic Absorption Spectroscopy. NH_4^+ ion was analyzed by Indophenol blue method using Varian UV spectrophotometer [*Tare et al.*, 2006].

[10] Size-segregated chemical data were analyzed for 12 days between 25 December 2004 and 7 January 2005 to calculate mass and number size distribution of each species. During this period, AERONET measurements coincide with the in situ measurements for 9 days, which allow us to compare our results with the AERONET data to assess the validity of our model. It should be noted, however, that our model is based on the real-time chemical measurements, whereas the AERONET retrievals [*Holben et al.*, 2001; *Dubovik and King*, 2000] are based on inverse modeling of the radiance reaching the surface.

3.2. Model Description

[11] From the chemical composition analyzed in Kanpur during land campaign II and in Agra during the monsoon season, it is evident that BC, $(NH4)_2SO_4$ (nss-SO_4), nitrate (NO_3^-), dust and K^+, Na^+, Cl^- (summed together and hereafter referred as salt) are the dominant aerosol components in the GB. Dust here is considered as either local soil-derived or industrial emission (mainly fly ash) and transported from far distances and estimated from the acid-soluble ion concentrations. The maximum, minimum and the mean values of the mass of each species in the fine and coarse mode fraction are listed in Table 1.

3.2.1. Aerosol Size Distribution

[12] The mass size distribution of all the species except BC as obtained from the in situ chemical data was fitted with bimodal log normal function according to the equation:

$$\frac{dM}{d\log r} = \sum_{i=1}^{n} \frac{M_i}{\sqrt{2\Pi}\log\sigma_i} \exp\left[\left(\frac{\log r - \log R_{m(h)i}}{\log\sigma_i}\right)^2\right]. \quad (1)$$

The microphysical parameters, mass mode radius at the ambient relative humidity ($R_{m\ (h),i}$) and geometric standard deviation (σ_i) of each individual species, in each mode *i*, determined from the distribution were then used to calculate number mode radius, $R_{n\ (h),\ i}$ by the relation [*Mallet et al.*, 2004]:

$$\log\left(R_{n(h),i}\right) = \log\left(R_{m(h),i}\right) - 3(\log\sigma_i)^2 \ln 10, \quad (2)$$

because the number distribution is required for calculation of optical properties using Mie theory. Here, it should be noted that σ_i remains same for both mass and number size distributions. As we do not have the in situ BC size spectra, we used the σ_i and $R_{n\ (h),i}$ values reported in OPAC model of *Hess et al.* [1998] for the same. The number size distribution parameters ($R_{n\ (h),i}$ and σ_i) for each species during each observational day are listed in Table 2. The

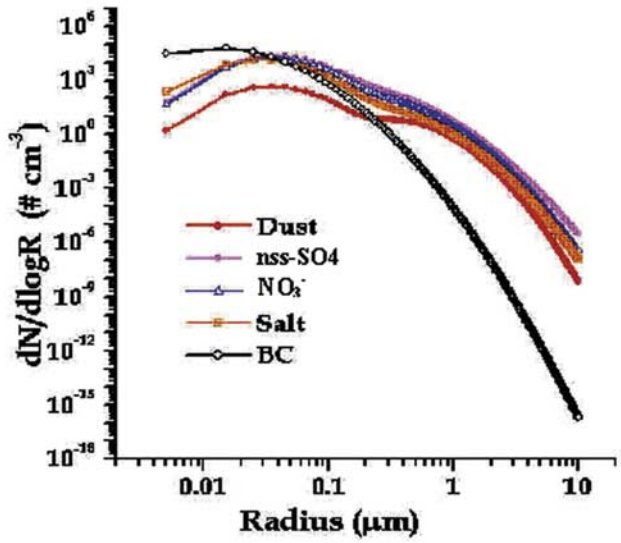

Figure 3. Mean number size distribution for each species during the observational period.

Table 2. Microphysical Parameters ($R_{mod(h)}$, σ) and Number Concentration (N) in Fine and Coarse Mode for Different Aerosol Species at Kanpur During the Campaign Period[a]

	Dates in December 2004 and January 2005												
Mode	25 (93)	26 (74)	27 (67)	30 (69)	31 (71)	1 (83)	2 (84)	3 (88)	4 (77)	5 (70)	6 (75)	7 (73)	Mean
						nss-SO_4							
Fine													
$R_{mod\ (h)}$	0.043	0.026	0.03	0.026	0.039	0.041	0.042	0.044	0.03	0.032	0.036	0.039	0.036 ± 0.01
σ	1.7	1.86	1.81	1.86	1.72	1.71	1.71	1.68	1.81	1.79	1.75	1.71	1.76 ± 0.06
N (*10)	2745	3822	3730	4390	4248	3607	3519	2280	2700	3675	3085	2502	3358.58
Coarse													
$R_{mod\ (h)}$	0.076	0.105	0.105	0.111	0.091	0.063	0.07	0.053	0.135	0.162	0.125	0.105	0.1 ± 0.03
σ	2.19	2.05	2.05	2.07	2.13	2.27	2.2	2.31	1.96	1.9	1.99	2.07	2.1 ± 0.12
N	2160	420	690	325	895	2600	2750	3340	325	214	360	440	1209.9
						NO_3^-							
Fine													
$R_{mod\ (h)}$	0.046	0.025	0.027	0.028	0.038	0.041	0.042	0.044	0.032	0.032	0.036	0.036	0.036 ± 0.01
σ	1.67	1.86	1.84	1.79	1.73	1.7	1.69	1.69	1.78	1.78	1.74	1.75	1.75 ± 0.06
N (*10)	1532	3213	3369	2934	3603	2919	2765	1716	1667	3099	2751	2388	2663
Coarse													
$R_{mod\ (h)}$	0.15	0.207	0.134	0.168	0.196	0.154	0.133	0.134	0.193	0.191	0.168	0.162	0.166 ± 0.03
σ	1.96	1.85	1.99	1.92	1.85	1.94	2.0	1.96	1.88	1.85	1.89	1.9	1.92 ± 0.05
N	208	400	200	152	155	285	400	360	74	95	130	132	215.92
						Dust							
Fine													
$R_{mod\ (h)}$	0.037	0.021	0.04	0.027	0.038	0.036	0.039	0.032	0.04	0.044	0.022	0.034	0.034 ± 0.01
σ	1.74	1.94	1.72	1.84	1.72	1.76	1.71	1.78	1.72	1.68	1.91	1.76	1.77 ± 0.08
N	254.4	1311	790	882	817	386.3	367.6	533.3	546	444	1083.5	409	652.01
Coarse													
$R_{mod\ (h)}$	0.284	0.284	0.345	0.329	0.379	0.319	0.274	0.321	0.284	0.251	0.237	0.295	0.3 ± 0.04
σ	1.77	1.77	1.66	1.69	1.67	1.71	1.66	1.71	1.75	1.76	1.82	1.74	1.72 ± 0.05
N	13.55	14	13	20.4	10.2	14.45	59.5	5.6	25.7	40	25	11	21
						Salt							
Fine													
$R_{mod\ (h)}$	0.028	0.019	0.028	0.021	0.028	0.3	0.3	0.034	0.022	0.043	0.024	0.027	0.028 ± 0.01
σ	1.81	1.9	1.83	1.88	1.83	1.8	1.81	1.76	1.9	1.69	1.89	1.84	1.83 ± 0.06
N (*10)	1820	3442	2205	3035	1921	1791	1957	1453	1896	806	2250	1440	2001.25
Coarse													
$R_{mod\ (h)}$	0.12	0.307	0.122	0.26	0.184	0.185	0.152	0.131	0.252	0.187	0.156	0.171	0.186 ± 0.06
σ	2.01	1.7	2.03	1.78	1.88	1.87	1.94	1.98	1.77	1.89	1.94	1.91	1.89 ± 0.1
N	142	10.2	77	11.7	42.5	56.8	88	90	10.1	25.5	33.8	27	51.22
						BC							
$R_{mod\ (h)}$													0.0118
σ													2.0
N (*10)	14300	6670	6368	10329	14329	16985	20400	19553	5171	9754	10408	6462	11729.1

[a] $R_{mod(h)}$ and σ represent mode radius at ambient humidity and the geometric standard deviation of the number size distribution. The corresponding RH for a day is listed in parentheses after that date. Note that number concentrations for BC and for nss-SO4, N, salt at the fine modes are listed as 1/10th of the original values.

corresponding mean (for all days) $R_{m\ (h),i}$ for nss-SO_4, NO_3^-, salt and dust in the fine and coarse modes are 0.092 ± 0.006 and 0.5 ± 0.04, 0.09 ± 0.008 and 0.584 ± 0.04, 0.082 ± 0.008 and 0.607 ± 0.07, 0.09 ± 0.008 and 0.727 ± 0.06, respectively. It is important to note here that the accumulation and coarse modes of a mass size distribution shift to the fine and accumulation modes, respectively of its corresponding number size distribution [*Whitby*, 1978]. The mean number size distribution for each species is depicted in Figure 3. All species except BC show bimodal distribution.

3.2.2. Mixing State of Aerosols

[13] To build a comprehensive aerosol model, we assume the aerosol species to be mixed externally. The optical computations by Mie theory were performed using the Optical Properties of Aerosol and Cloud (OPAC) model [*Hess et al.*, 1998] at 0.35, 0.45, 0.5, 0.55, 0.65, 0.8, 0.9 and 1.025 μm wavelengths. The extinction coefficient ($b_{ext,i}$) and scattering coefficient ($b_{sca,i}$) of each species were computed at different RH (0, 50, 70, 80, 90 and 95%) to account for the humidification effect. The optical properties of BC and dust remain unchanged as they are considered nonhygroscopic in nature. Single scattering albedo (SSA, ω_0) and the asymmetry parameter (g) of the composite aerosol were then derived from the following relations:

$$\omega_0 = \frac{\sum_i b_{ext,i}\omega_{0,i}}{\sum_i b_{ext,i}} \quad (3)$$

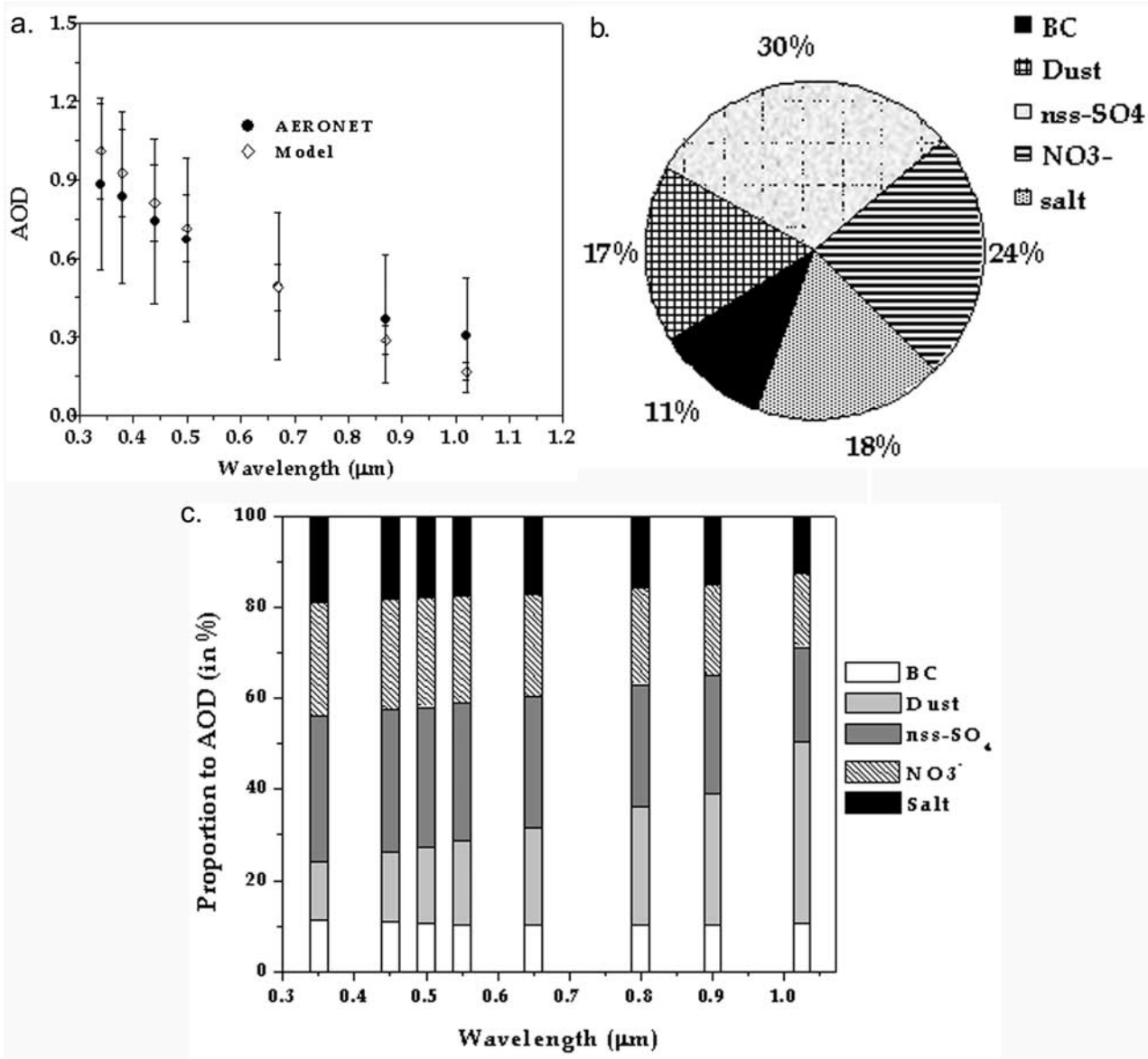

Figure 4. (a) Comparison of model-estimated spectral AOD with AERONET measurements. Vertical bars represent the standard deviations from the mean values represented by the points. (b) Relative proportion of various components to the composite $AOD_{0.5}$. (c) Wavelength-dependent relative share of the various components to the composite AOD. (d) Change in b_{sca} and b_{abs} (at 0.5 μm) for the fine (b_{scaf} and b_{absf}) and coarse (b_{scac} and b_{absc}) mode fractions with RH (see the text for details). The b_{scaf} is plotted in the primary *Y* axis and the other three parameters are plotted in secondary *Y* axis. Note that the scales of two *Y* axes are different. (e) Contribution of fine and coarse mode fractions to the scattering and absorption at 0.5 μm. Here, "b_{scaf}," "b_{absf}," "b_{scac}" and "b_{absc}" denote scattering coefficient of fine mode, absorption coefficient of fine mode, scattering coefficient of coarse mode and absorption coefficient of coarse mode fractions, respectively. b_{absf}, b_{scac} and b_{absc} are drawn in secondary *Y* axis. A sharp rise is observed at RH = 80% for b_{scaf}, which is marked as deliquescence point for hygroscopic particles in fine mode fraction. (f) Wavelength-dependent absorption coefficient of the composite aerosol. The mean values are fitted with a power law relation. The vertical bars through the mean values are the respective standard deviations.

and

$$g = \frac{\sum_i b_{sca,i} g_i}{\sum_i b_{sca,i}}. \quad (4)$$

[14] From the BC number size distribution, we have found that 90% BC particles lie in the fine mode fraction, which we have considered during further computations of the optical properties for the fine and coarse mode fractions

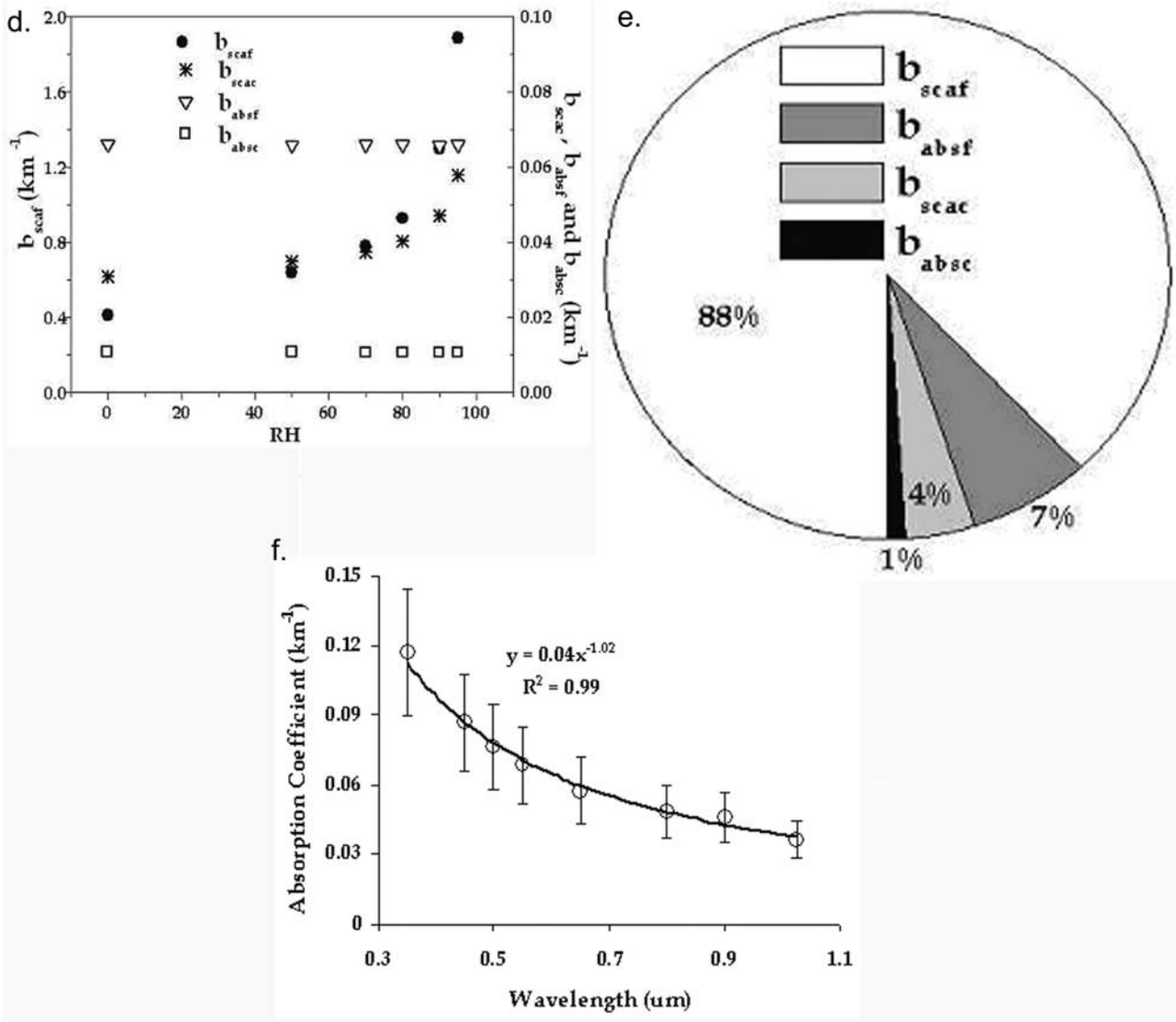

Figure 4. (continued)

separately, which is important to assess the anthropogenic contribution.

4. Aerosol Characteristics

4.1. Aerosol Optical Depth

[15] Spectral AOD for the composite aerosol was computed from the b_{ext}values. As, we do not have real-time vertical profile of aerosols, we assume that the distribution of aerosols in vertical column would be similar to the BC profile derived from aircraft measurements during January 2005 [*Tripathi et al.*, 2005b], which shows that most of the particles are present within the boundary layer. The measured BC concentration at different altitudes was fitted in OPAC model to estimate the BC number concentration at the corresponding heights. Using this information, we have calculated the scale height (~1.2 km), which has been assumed similar for all the species, as no information is available for the scale heights of different species in Indian region. The modeled spectral AOD, which is the sum of the AOD by each individual species, was compared with the simultaneous measurements by ground-based CIMEL radiometer (Figure 4a). For direct comparison with AERONET, the AOD values are estimated at the same wavelengths from the model-derived AOD spectra using nonlinear interpolation [*Tripathi et al.*, 2005a]. The vertical bars through each point are the standard deviations of the mean values for the observational period. Although the model-derived AOD spectrum is steeper than AERONET-derived AOD spectrum, the estimated values are within $\pm 1\sigma$ of the measured values during the study period. The underestimation at the higher wavelengths could be either due to the presence of some missing components aloft, which were not collected at the surface or some components not analyzed from the filter papers in the coarse mode. The unimodal BC size distribution taken from OPAC might increase the steepness of AOD spectrum, as it is mostly confined in the fine mode fraction.

[16] The relative share of each species to the composite AOD at 0.5 μm is illustrated in Figure 4b. Contribution of

Table 3. Fitting Parameters for Humidification Factors of Aerosols at Fine and Coarse Mode[a]

Wavelength, μm	Fine Mode		Coarse Mode, h
	a	b	
0.35	1.3	2.74	0.41
0.45	1.31	2.88	0.41
0.5	1.32	2.94	0.4
0.55	1.33	3	0.39
0.65	1.33	3.06	0.37
0.8	1.34	3.12	0.34
0.9	1.34	3.14	0.31
1.025	1.33	3.11	0.22

[a]Note that the fitting equations for fine and coarse modes are different.

nss-SO_4 (30%) to the $AOD_{0.5}$ is maximum, followed by NO_3^- (24%), salt (18%), dust (17%) and BC (11%). The contribution of the hygroscopic components (nss-SO_4, NO_3^- and salt) is dominated by the fine mode fraction ($\sim$90%), whereas for the mineral dust, the contribution by fine ($\sim$54%) and coarse mode ($\sim$46%) are comparable. The F_{BC} during the observation period varied from 5 to 10%. On average, $\sim$8% F_{BC} contributes 11% to the observed optical depth in Kanpur, whereas over the Indian Ocean, 6% F_{BC} contributed $\sim$11% to the AOD [*Satheesh et al.*, 1999]. This difference can be explained by the effect of RH on the b_{ext} of the composite aerosol, as in presence of high ambient RH, the scattering by the fine mode fraction is enhanced because of the hygroscopic growth. Hence the relative percentage of b_{sca} to b_{ext} increases, as b_{abs}remains unchanged. This effect is more conspicuous in case of internal mixing as in that case, each particle will contribute to the increase in b_{sca}. The role of RH in the estimated radiative forcing is discussed in details later on.

[17] The contribution of each component to the optical depth was found to vary with wavelength (Figure 4c). nss-SO_4, NO_3^- and salt show a decreasing trend (reduction of 11, 9 and 7% relative contribution, respectively), whereas the relative contribution of dust increases from 13 to 40% at the highest wavelength. This shows the significant impact of dust on the aerosol optical property at the higher (near infrared) wavelengths. BC contribution, on the contrary is spectrally insensitive.

4.2. Effect of Relative Humidity on the Optical Property

[18] To account for the effect of RH on the growth of the particles and subsequently on b_{ext}, the wavelength-dependent humidification factor, f(RH), was determined. f(RH) (= $b_{ext,RH}/b_{ext,dry}$); signifies the increase in b_{ext}due to enhanced scattering by hygroscopic particles at higher RH as compared with dry-state extinction coefficient, $b_{ext,dry}$. The scattering (b_{sca}) and absorption coefficient (b_{abs}) at 0.5 μm in the fine and coarse mode fractions at different RH are shown in Figure 4d. It is clear that only the scattering coefficient of fine mode fraction shows strong hygroscopic growth, with a sharp change in the curve at around 80% RH (deliquescence point for the hygroscopic components). The scattering coefficient of coarse mode particles display moderate increase, whereas, b_{abs} at fine and coarse mode show no variation.

[19] The b_{ext} values (sum of b_{sca} and b_{abs}) at ambient RH for each observational day for fine mode fraction were fitted in the modeled equations:

$$b_{ext,RH} = b_{ext,dry}\left(1 + a(RH/100)^b\right), \quad (5)$$

whereas, the coarse mode particles were best fitted with an equation of form:

$$b_{ext,RH} = b_{ext,dry}\left(1 - (RH/100)^{-h}\right). \quad (6)$$

Here, "a," "b" and "h" are empirical fitting parameters and their values at each wavelength are listed in Table 3. *Kotchenruther et al.* [1999] have shown that equation (5) is best suited for the particles showing deliquescent behavior, whereas, equation (6) captures the nature of moderate hygroscopic growth.

[20] The fine mode fraction shows higher rate of hygroscopic growth compared to the coarse mode fraction, which is not surprising. The rate of increase of the surface area is much higher for the fine mode fraction, which enhances the light scattering. These relations are important in the context of the parameterization of AOD in terms of the mass of the chemical species.

4.3. Parameterization of AOD

[21] Aerosol optical property is primarily and most commonly represented by AOD, which can be measured by ground-based radiometer and satellites. AOD depends on the aerosol chemical composition and its vertical distribution. Even to study the aerosol burden and their radiative effects, AOD data are most important and widely available (at least the satellite data product), whereas, the chemical composition data are scanty. In the GB, hence we tried to derive a generalized expression for AOD in terms of the mass concentration of the species at the surface.

[22] The resulting AOD at 0.5 μm was parameterized in the form of:

$$AOD_{0.5} = a_0 + \sum_{i=1}^{6} a_i e_i f(RH)[i]c_i. \quad (7)$$

Here, a_0 is the intercept (0.35978) and a_i is the regression coefficients of ith species (values are listed in Table 4). e_i and $[i]$ are the dry mass extinction efficiency and mass concentration of ith species, respectively and c_i is inverse of the percentage contribution of ith species to $AOD_{0.5}$. It is important to account the hygroscopic growth of nss-SO_4,

Table 4. Coefficients of Parameterization of AOD[a]

Species	a_i	f(RH)	e_i
nss-SO_4	0.00825	2.03 ± 0.46	3
$N0_3^-$	0.0056	2.03 ± 0.46	3
Salt	0.00797	2.03 ± 0.46	3
BC	0.07669	1	10
$(Dust)_f$	0.07042	1	1
$(Dust)_c$	0.00111	1	0.6

[a]Unit of e is in $m^2\ g^{-1}$. The subscripts "f" and "c" denote the fine and coarse mode fractions, respectively.

NO_3^- and salt, therefore estimated values of f(RH) for the water-soluble components were used. f(RH) for BC and dust is 1, as $b_{ext}$for these species does not change with RH. e_i values for different species (Table 4) were taken from *Malm et al.* [1994].

[23] The regression relation suggests that the surface concentrations of the major aerosol components are able to reproduce 76% of the observed AOD with a root mean square error of 0.134. The rest 24% is attributed to the components in the atmospheric column and some minor species, which were not analyzed. RH has been found to play a significant role in changing the composite aerosol optical property in the region, as without considering f(RH), the regression coefficient comes down to 0.53.

4.4. Relative Contribution of Fine and Coarse Mode Fraction

[24] The observed b_{ext} and subsequently the optical depth account for both natural and anthropogenic contribution. The natural emission during the winter season mainly coming from the soil is much less compared to that during the summer season, when the dusts transported from the desert regions in the western India and the Middle East Asia add to the local crustal emissions [*Dey et al.*, 2004; *Chinnam et al.*, 2006]. The fine mode fraction of AOD is very high (more than 90%) over the entire GB during the winter season, as observed by MODIS data [*Jethva et al.*, 2005]. *Tare et al.* [2006] using the tracer technique has shown that during the campaign, the contribution of soil-derived components to the measured mass is mostly confined in the coarse mode fraction. In the fine mode fraction, soil-derived components (i.e., fine mode dust) contribute only ~4%. Besides, fine mode dust, natural organics from biogenic emissions (not measured) could contribute to the fine mode fraction. In general, except dust, all other species are either emitted directly from anthropogenic activities or formed in the atmospheric from precursor gases emitted from anthropogenic sources. Even, the biomass burning in this region is not natural; rather they are anthropogenic. Ignoring the contribution from natural organics, the anthropogenic contribution to the AOD has been estimated to be maximum ~83%. *Ramanathan and Ramana* [2005] have reported that the anthropogenic contribution in the GB during the dry season is 70–80%.

[25] Figure 4e depicts the relative contribution of scattering and absorption by the fine and coarse mode fraction to the total extinction. From the model, we have found that the fine mode fraction contributes 95% (88% and 7% accounts for the scattering and absorption respectively) to the total extinction. The rest 5% contribution comes from the coarse mode fraction, where the ratio of scattering to absorption is 4:1. Another notable finding, coming out of these results is that, although the contribution of absorption by coarse mode fraction is lowest, it results in very low SSA (<0.85). *Dey et al.* [2005] from AERONET data have shown that over Kanpur, SSA at the fine (ω_f) and coarse (ω_c) mode, show maximum difference during the winter season. This aspect will be discussed in the next section.

[26] The absorption by the fine mode fraction is mainly attributed to the BC particles. The absorption coefficient (b_{abs}) estimated from the model has been fitted by a power law relation with wavelength (Figure 4f) in the form of:

$$b_{abs} = K\lambda^{-a_{abs}}, \tag{8}$$

where K is a fitting parameter and a_{abs} is absorption Ångström exponent. The value of a_{abs} was found to be 1.02. In the literature, many studies regarding the wavelength-dependent absorption of BC have been conducted. *Schnaiter et al.* [2003] have shown that the diesel-soot particles have a wavelength dependence of λ^{-1}, whereas, biomass burning causes a wavelength dependence of λ^{-2} [*Kirchstetter et al.*, 2004]. During the land campaign, in the southern India, *Ganguly et al.* [2005b] have found a value of 1.52 for a_{abs}, which was attributed to biofuel emission in association to fossil fuel burning. a_{abs} value for residential biofuel-derived BC varies between 1 and 2.9 [*Bond*, 2001]. Comparing our results with the existing literature, the main probable source of BC in this region has been inferred to be fossil fuel. Although organics were not measured in the campaign, the spectral variation of b_{abs} suggests that absorbing organics are not significant in terms of optical properties. However, the nonabsorbing organics may be present in the region, but because of lack of the data, no definite comment can be made on their role in modifying the optical properties. Recently, *Garland et al.* [2005] have experimentally shown that internally mixed insoluble organics and nss-SO_4will not change the water uptake capability of pure nss-SO_4 significantly, which means the optical properties will also not be affected greatly.

5. Single Scattering Albedo (ω_0) and Asymmetry Parameter (g)

[27] ω_0, which indicates the relative contribution of scattering and absorption to the total extinction by aerosols, is an important input to the radiative forcing calculation. ω_0 and g values derived for each observational day are illustrated in Figure 5a. The model-estimated SSA and g (at 0.55 μm wavelength) lie within the uncertainty of the AERONET measurements for most of the days, which proves that despite some discrepancy in AOD, the model is able to estimate the optical properties governingthe radiative forcing quite well. The mean $\omega_{0,0.55}$ for the composite aerosol comes out to be 0.92 ± 0.02, whereas the corresponding value for g is 0.7 ± 0.01.

[28] We have investigated the spectral variation of ω_f and ω_c to find a reasonable answer to the observations by *Dey et al.* [2005], where they have found large difference in ω_f and ω_c during the winter season. The model- and AERONET-derived spectral ω_f and ω_c are plotted in Figure 5b. In the fine mode fraction, the modeled ω_f shows higher spectral dependence (varying from 0.93 at 0.35 μm to 0.85 at 1.025 μm) compared to the AERONET values. However, the model results show excellent match (maximum difference of ~3.5%) with the AERONET observations in the coarse mode fraction. The spectral variation of ω_f and ω_c are opposite. As the absorption Ångström exponent (a_{abs}) is less than the Ångström wavelength exponent (i.e., spectral dependence of AOD, $\alpha \sim 1.4$), ω_0 should decrease with wavelength [*Bergstrom et al.*, 2004]. This is reflected in the model-derived ω_0 spectra in fine mode fraction. However,

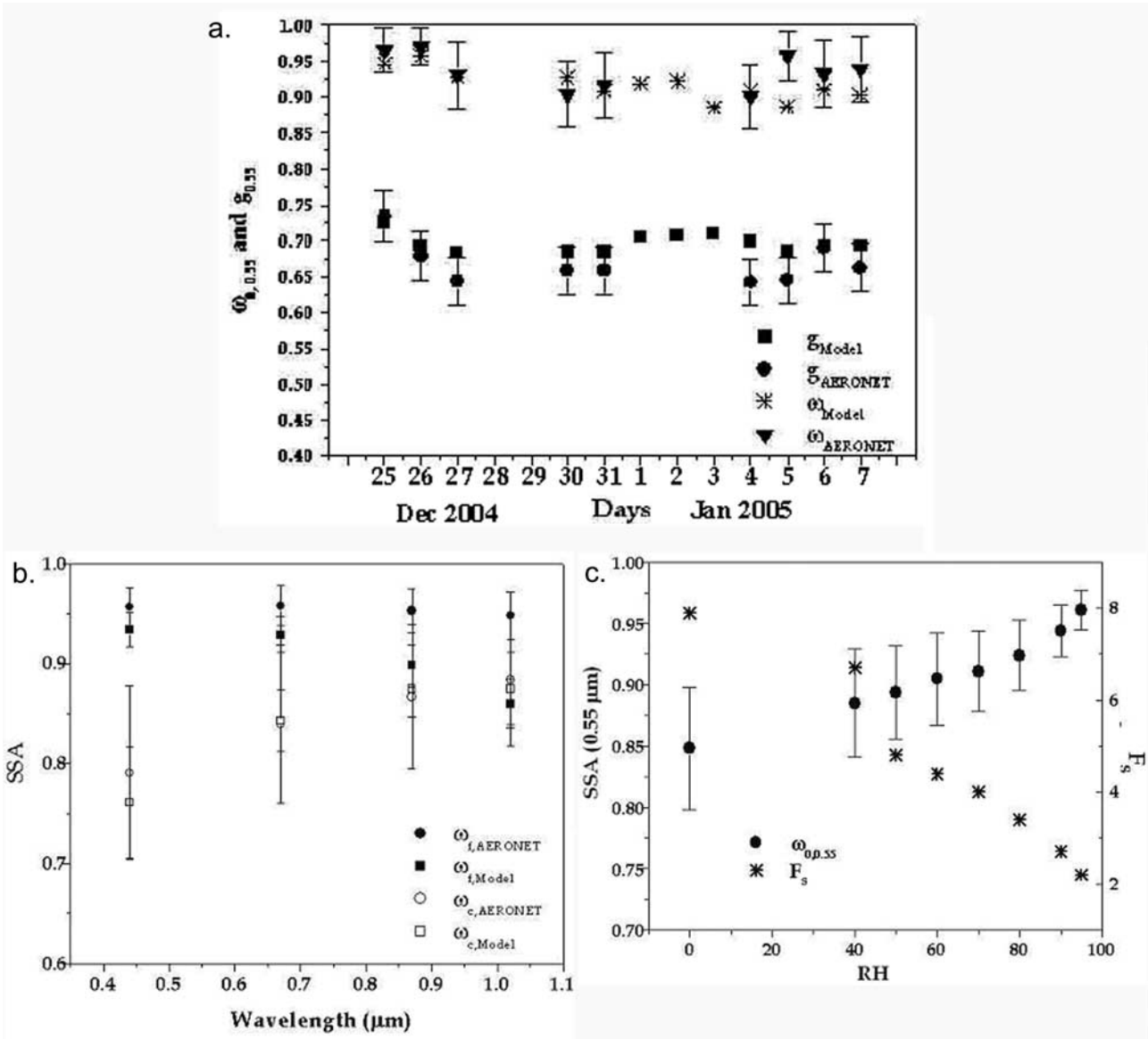

Figure 5. (a) $\omega_{0,0.55}$ and $g_{0.55}$ deduced from AERONET observations and estimated from the model for each observational day. The AERONET retrieval error is shown as error bar. (b) Spectral dependence of $\omega_{0,0.55}$ in the fine and coarse mode fractions as derived from the model estimates and AERONET measurements. (c) Variation of $\omega_{0,0.55}$ and F_S for the composite aerosol model with RH. The vertical bars through each point (mean) are the standard deviations for the observational period. F_S indicates the ratio of surface aerosol forcing to TOA aerosol forcing.

the higher spectral variation of ω_f in the model results from higher difference in α and a_{abs} in case of the model-derived values than the AERONET measurements, as the model-derived α is higher than AERONET-retrieved α (as shown by AOD spectra in Figure 4a). Also, it should be noted that the derivation of ω_0 spectral variation is different for model (direct estimate by Mie theory from surface mass concentration) and AERONET retrieval (inverting the direct and diffuse sky radiance for the atmospheric column). On the other hand, in the coarse mode fraction, ω_0 has been found to increase with wavelength (varying from 0.715 at 0.35 μm to 0.882 at 1.025 μm). The increase in ω_c with wavelength suggesting more absorption at the lower wavelengths implies that the ω_c is dominated by the dust particles [*Dubovik et al.*, 2002].

[29] Low ω_c values cannot be due to mineral dust alone. *Dubovik et al.* [2002], from AERONET measurements near the desert sites, have shown that although the dust ω_0 increases with wavelength, the values generally lie above 0.9. It is understandable that the dust absorption, which occurs primarily because of the iron oxides (or hematite), is one of the most uncertain parameter to model. *Sokolik and Toon* [1999] from model calculations have found that even for 20% hematite, $\omega_{0,0.55}$becomes ~0.9. In the GB, the Fe content in the local soil-derived dust during the winter season is much less than that during the summer season,

when desert dusts are being transported to GB [*Chinnam et al.*, 2006]. The observed excess absorption in the coarse mode is attributed to mixing of BC particles with the dust. This is confirmed by the fact that if all BC particles are removed from the coarse mode, $\omega_{c,0.55}$ becomes 0.92 with similar increasing spectral trend. The mixing of BC and dust at the coarse mode fraction could be internal, where the BC particles get attached on the surface of dust particles enhancing the absorption efficiency [*Clarke et al.*, 2004].

[30] Another important aspect to be considered here is the RH, as ω_0 has been found to be sensitive to the RH. For RH below 60%, $\omega_{0,0.55}$ dips down below 0.9 (Figure 5c), indicating less scattering and higher relative contribution of absorption to the total extinction. Earlier work by *Ramanathan and Ramana* [2005] has confirmed the presence of absorbing brown cloud over the entire GB. In fact, because of enhanced scattering by fine mode fraction (Figure 4d) with increase in RH, the relative contribution of BC absorption becomes less. This observation is important, because during the foggy/hazy days, RH becomes high over the GB. This means even if absorbing aerosols are present in high concentration, it will not be truly reflected on the net effect on the radiative forcing.

6. Implications to Radiative Forcing

[31] Aerosol radiative forcing at both top of the atmosphere (TOA) and surface (S) has been estimated from the difference in values calculated for the aerosol-free F (na), and aerosol-laden F (a), atmosphere, which can be represented as [*Moorthy et al.*, 2005a]:

$$\Delta F_{TOA/S} = F(na)_{TOA/S} - F(a)_{TOA/S}. \quad (9)$$

The atmospheric forcing (ΔF_{atm}) is defined as the difference of ΔF_{TOA} and ΔF_S. The aerosol radiative forcing depends on many factors such as aerosol composition and optical properties, atmospheric condition, cloud properties, surface albedo. Here we have considered clear-sky condition to estimate the aerosol radiative forcing in the shortwave (SW, 0.25–4 μm) and longwave (LW, 4–100 μm) wavelength region.

[32] Santa Barbara Discrete Ordinate Radiative Transfer (SBDART) model developed by *Ricchiazzi et al.* [1998] has been used to estimate the aerosol radiative forcing. SBDART is a plane-parallel radiative transfer code based on the discrete ordinate approach and has been used by many investigators to estimate aerosol radiative forcing. The radiative transfer equations are numerically integrated with Discrete Ordinate Radiative Transfer (DISORT) module [*Stamnes et al.*, 1988] in the SBDART. This method uses numerically stable algorithm to solve the equations of plane-parallel radiative transfer in vertically inhomogeneous atmosphere [*Ricchiazzi et al.*, 1998]. In SBDART, the intensity of scattered and thermally emitted radiation can be computed at different directions and heights. Computations can be performed up to 65 atmospheric layers and 40 radiation streams. To account molecular absorption, SBDART relies on low-resolution band models developed for LOWTRAN 7 atmospheric transmission code [*Pierluissi and Peng*, 1985]. This code provides clear sky atmospheric transmission from 0 to 50000 cm^{-1}, which includes the effects of all radiatively active molecular species in the Earth's atmosphere with a wavelength resolution of 5 nm in the visible and 200 nm in the infrared region.

[33] The input parameter required for DISORT module in SBDART are spectral extinction optical depth (τ_a), ω_0 and g (i.e., intensity-weighted average of the cosine of the scattering angle). The scattering phase function required for radiative transfer computations is generated from the asymmetry parameter using the Heyney-Greenstein approximation. Spectral τ_a, ω_0 and g, calculated from the measured chemical data through the OPAC model assuming external mixing were incorporated in the SBDART model. *Pilnis et al.* [1995] have shown that the aerosol direct radiative forcing is not much sensitive to the state of mixing. ΔF_{TOA} and ΔF_S were estimated for solar zenith angle (SZA) at every 5° interval and the diurnally averaged forcing ($\Delta F_{TOA/S}$) were calculated by:

$$\Delta F = \frac{1}{2}\int_0^1 \Delta F(\mu_0) d\mu_0, \quad (10)$$

where, μ_0 is the cosine of the SZA. Surface albedo is an important input parameter in the radiative forcing calculation [*Satheesh*, 2002b]. *Satheesh et al.* [2002] have shown that if the INDOEX model was used over land (having higher surface reflectance), TOA forcing becomes positive from negative over ocean and the atmospheric forcing increases by 7 W m^{-2}. We have considered the same surface albedo value (derived from MODIS data), which was used by *Tripathi et al.* [2005c] for estimating BC radiative forcing during the winter season at Kanpur. During the observational period, SW TOA and surface forcing due to aerosols vary in the range −7.6 to −18.8 W m^{-2} and −30.9 to −58.4 W m^{-2} (Figure 6a), respectively, with corresponding mean values of −12.7 ± 3 and −43 ± 8 W m^{-2}. The LW TOA and surface forcing (Figure 6b) vary in the range +2.4 to +5.1 W m^{-2} and +2to +4.4 W m^{-2}, respectively, with corresponding mean values of +3.6 ± 0.7 and +2.9 ± 0.6 W m^{-2}. The mean SW and LW surface forcing efficiency are −71.9 ± 19 and +5 ± 1.5 W m^{-2} per unit optical depth, whereas the corresponding TOA forcing efficiency are −25.3 ± 10 and 6.1 ± 1.8 W m^{-2}, respectively. The resulting net atmospheric forcing due to SW and LW comes out to be +31.3 ± 9.2 W m^{-2}.

[34] The net positive radiative flux, which is absorbed in the atmosphere, gets transformed into heat. The heating rate of the atmosphere is defined as [*Liou*, 2002]

$$\frac{\partial T}{\partial t} = \frac{g}{C_p}\frac{\Delta F_{atm}}{\Delta P}, \quad (11)$$

where $\delta T/\delta t$ is the heating rate, C_p is the specific heat capacity of air at constant pressure, g is the acceleration due to gravity and P is the atmospheric pressure. The resulting heating rate for the atmosphere comes out be 0.9 ± 0.3 K day^{-1} over Kanpur. The heating rate during the observational period varies from 0.52 to 1.35 K day^{-1}. *Tripathi et al.* [2005c], from one month (December 2004) measurements, estimated that the atmospheric forcing (+71 W m^{-2}) over Kanpur due to BC, was very high and the TOA (+9 W m^{-2}) forcing becomes positive. Our results suggest that,

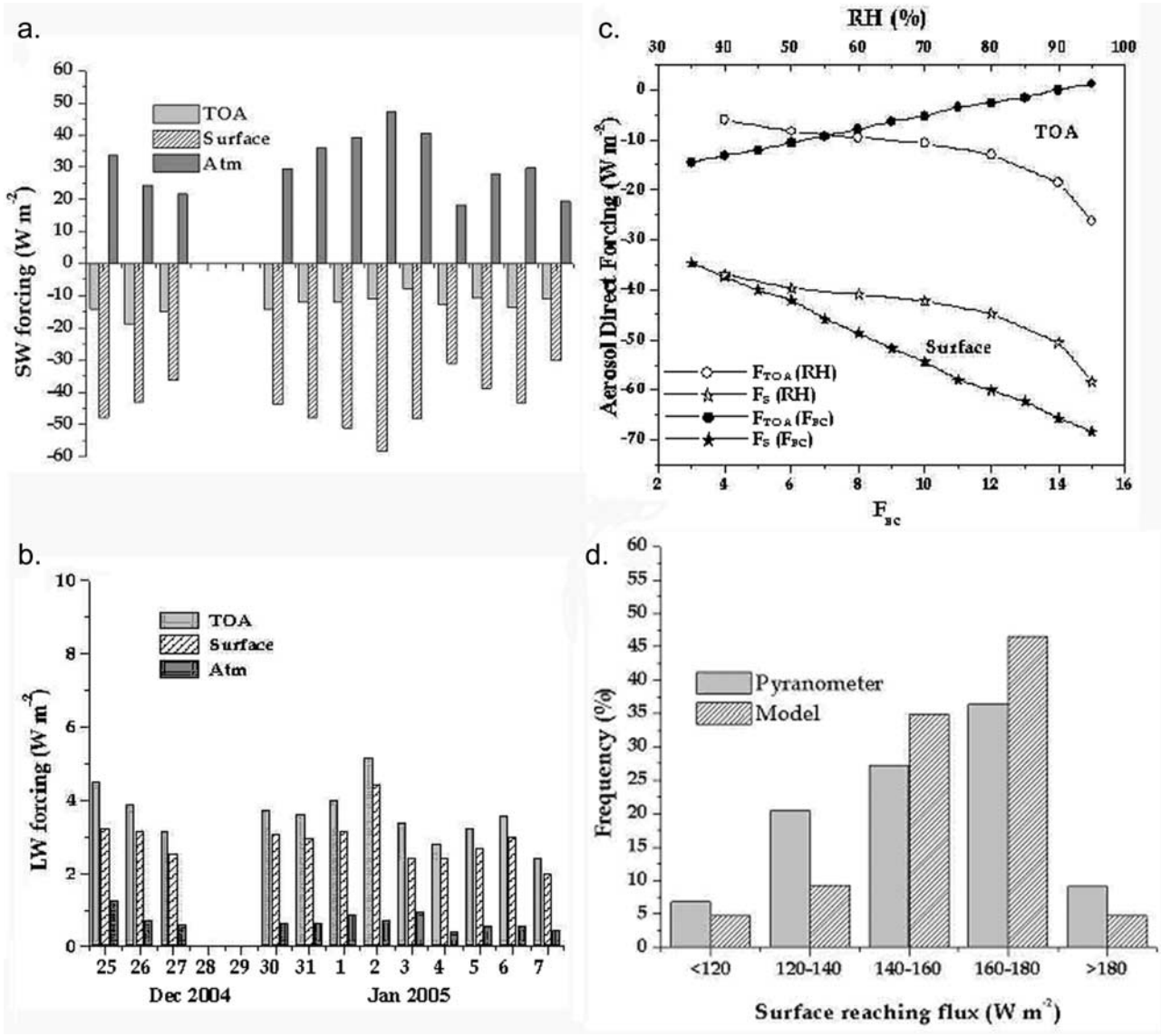

Figure 6. (a) Shortwave clear-sky radiative forcing (in W m^{-2}) at the TOA, surface and atmosphere for each observational day. (b) Same as Figure 6a but for longwave region. (c) Variations of the TOA (circle) and surface (star) forcing with the BC mass fraction, F_{BC} (solid circle and star) and RH (open circle and star). The sensitivity of the forcing with F_{BC} is estimated at RH = 70% and the sensitivity of forcing with RH is estimated at F_{BC} = 6%. (d) Frequency distributions of surface reaching flux as measured by Pyranometer and estimated from the model.

although the net atmospheric absorption reduces considering all the major components, still the absorption is significant as compared with the INDOEX results, where the atmospheric heating rate was estimated to be ~0.5 K day^{-1} [*Satheesh et al.*, 2002].

[35] As, the aerosol optical properties show strong RH dependence, the aerosol radiative forcing also vary with RH accordingly. We have found that the SW forcing is much more sensitive to RH compared to the LW forcing. Both SW surface and TOA forcing and hence their ratio (F_S, indicating the amount of absorbing aerosols [*Satheesh and Ramanathan*, 2000]) is found to decrease with increasing RH (Figure 5c). This is also indicated by the variation of SSA with RH shown in same plot. The absorbing species in our model are BC and dust, whose contribution to the total extinction is suppressed at the higher RH, resulting in higher TOA and surface cooling. However, the rate of increase of TOA forcing ($\Delta F_{TOA}/\Delta RH$ ~0.23 W m^{-2}) is less compared to that for surface forcing ($\Delta F_S/\Delta RH$ ~0.25 W m^{-2}), leading to decrease in F_S. $F_S$decreases very rapidly up to 50% RH, after which the rate of decrease becomes less. The variation of F_S with RH depends on the relative proportion of the absorbing and nonabsorbing components, as the model study by *Podgorny et al.* [2000] have shown that absorbing species contribute more to the surface forcing, while the nonabsorbing species contribute more to TOA forcing. Over Kanpur, F_S varies between 2.7 to 10.8 with a mean value of 5 ± 2.5, which is 40% higher than the INDOEX observations [*Satheesh et al.*, 2002].

[36] In order to apply our model for the GB, we have performed a sensitivity test for the TOA and surface forcing within the realistic range of RH and F_{BC}, as these two parameters having most significant impact on the radiative forcing, could vary spatially. The variations of the TOA and the surface forcing with RH (varying in between 40 and 95%) and F_{BC}(varying in the range 3–15%), are shown in Figure 6c. TOA forcing shifts from negative to near zero/positive and the surface forcing shifts toward more negative values with increase in F_{BC}, as higher BC concentration enhances the absorption in the atmosphere and contributes to more surface cooling. In contrast, at higher RH, both TOA and surface forcing show more negative values, implying the significance of enhanced scattering by hygroscopic particles. Although, the atmosphere forcing is much less sensitive to RH ($\Delta F_{atm}/\Delta RH \sim 0.03$ W m^{-2}) than to F_{BC}($\Delta F_{atm}/\Delta F_{BC} \sim 4$ W m^{-2}), the RH effect is best reflected in the variation of F_S (Figure 6c).

7. Uncertainties in the Estimation of the Radiative Forcing

[37] The aerosol direct radiative forcing has been estimated for Kanpur using the model-derived optical properties in SW and LW wavelength regions. Numerous factors influence the aerosol optical properties and hence the forcing, e.g., size distribution and scale height of each species, state of mixing, RH, F_{BC}, surface albedo and sky condition (clouds). Here, all the forcing values are reported for clear-sky conditions assuming similar scale height for all the species. Information about individual scale height for each species is not available in the Indian region. We have seen that reduction of scale height (e.g., if the INDOEX value is chosen) reduces $AOD_{0.5}$ by ~10% along with flattening of AOD spectrum. However, in that condition, surface forcing was estimated to be higher by 2 W m^{-2} (than the present case) and TOA forcing is lower by ~2.6 W m^{-2}. In our model, besides BC, the size distributions of other four components were derived from measured mass size distribution. BC size distribution was taken from OPAC, which may induce some error in the estimated optical properties, if it does not match with the actual BC size distribution in this region. An increase of 20% in the R_{mod} of BC size distribution increases the composite SSA and g (at 0.5 μm) by ~2 and 0.4%, respectively and decreases the composite $AOD_{0.5}$ by 5.8%. This would induce an error of 5% on the TOA and surface forcing estimation.

[38] We extended our model over the entire GB assuming that the emission factors of pollutants are not significantly different in spatial scale over the GB [*Reddy and Venkataraman*, 2002a, 2002b]. We have tested the sensitivity of TOA and surface forcing due to RH and F_{BC} and found that the variation of F_{BC} would induce larger error than the variation of RH. *Reddy and Venkataraman* [2000] from model calculations have shown that BC contributes 5% to the annual aerosol burden in India. During the winter, average F_{BC} in Kanpur was found to be ~10% [*Tripathi et al.*, 2005c], in Nainital, it was ~5% [*Pant et al.*, 2006]. There is no estimate of spatial variation of F_{BC} in GB, hence we have estimated the aerosol forcing using an average F_{BC} of 6%. 1% increase in F_{BC} would increase the TOA forcing by 1.3 W m^{-2} and decrease the surface forcing by 2.8 W m^{-2}. Another factor that may affect the aerosol radiative forcing is the mixing state. *Jacobson* [2000] has shown that the internally mixed aerosols could exhibit higher absorption than the externally mixed aerosols. On the other hand, many researchers [*Pilnis et al.*, 1995; *Hignett et al.*, 1999] have shown that the mixing state is not so important during the estimation of the total extinction. *Satheesh et al.* [2002] have shown that the mixing state did not change any conclusions of INDOEX model. In the real scenario, aerosols most likely exist in a state somewhere between externally mixed and internally mixed. However, if the internal mixing exists in form of core-shell configuration, the radiative impact could be different [*Chandra et al.*, 2004; *Jacobson*, 2000]. The exact nature of the mixing state of ambient aerosols in the GB is still unknown and need to be explored in future.

[39] MODIS-derived surface albedo value can have an average of 6% error in the SW region [*Strahler et al.*, 1999], which will induce ~3.5 and 1.5% error in the estimated TOA and surface forcing, respectively. *Pilnis et al.* [1995] have shown that single most important parameter influencing the direct forcing is RH (if the composition of aerosols remains more or less constant), as it strongly affects the hygroscopic components. We have used model-derived RH-dependent forcing efficiency values to estimate TOA and surface forcing in the GB. *Satheesh and Ramanathan* [2000] have shown that the forcing calculated using the efficiency values are not influenced by model offsets. However, the error in the estimated aerosol forcing efficiency due to the factors discussed above would propagate, as the model is extended spatially and temporally for the GB. The overall uncertainty in the estimation of TOA and surface forcing due to all these factors is worked out to be ~15%.

[40] A Kipp and Zonen pyranometer deployed in IITK under Solar radiation Network (http://solrad-net.gsfc.nasa.gov/) provides total solar irradiance data from September 2005 onward. Although, it was not possible to directly compare the model-estimated surface radiative flux with the measurements, we have compared the frequency distributions (Figure 6d) of the modeled and measured flux for the winter season. The level 1.0 data of pyranometer-measured surface reaching flux (measured in MJ m^{-2} day^{-1}) in an aerosol-laden atmosphere during December 2005 to January 2006 was converted to W m^{-2}. The average surface forcing efficiency calculated from the model using chemical data during the observational period and $AOD_{0.5}$ measured by AERONET were used to estimate the surface reaching flux in each day in the winter season (December 2004 to January 2005). The frequency distributions reveal that almost 90% data falls within 120–180 W m^{-2} range. Considering the fact that the absolute error in pyranometer-measured flux could be as high as 10 W m^{-2} [*Satheesh et al.*, 1999], and the data level is 1.0, which is not quality assured, at least, it can be commented that the model-derived fluxes lie in the similar range with the measured fluxes.

8. Applicability of the Model for the GB

[41] We have considered an average of 70% RH and 6% F_{BC} during the winter season to estimate the aerosol forcing

Table 5. TOA, Surface and Atmosphere Forcings Over the Major Cities in the GB and the Adjacent Oceanic Regions[a]

Area	Period	TOA	Surface	Atmosphere	Comments (Reference)
Kanpur	Dec–Feb	−9.1	−40.4	+31.3	urban, SW + LW (this study)
Delhi	Dec–Feb	−8.1	−39.6	+31.5	urban, SW + LW (this study)
Agra	Dec–Feb	−9	−42.5	+33.5	urban, SW + LW (this study)
Allahabad	Dec–Feb	−9.5	−44.3	+34.8	urban, SW + LW (this study)
Varanasi	Dec–Feb	−10.4	−49	+38.6	urban, SW + LW (this study)
Patna	Dec–Feb	−10.2	−47.9	+37.7	urban, SW + LW (this study)
Kolkata	Dec–Feb	−9.6	−46.2	+36.6	urban, SW + LW (this study)
GB	Dec–Feb	−6.4	−30.2	+23.8	SW + LW (this study)
GB	Dec–Feb	−8.6	−32	+23.4	SW (this study)
GB	Oct–May	∼0	−32	+32	SW [*Ramanathan and Ramana*, 2005]
Bangalore	Nov–Dec	+5	−23	+28	urban, SW [*Babu et al.*, 2002]
Pune	Nov–Apr	0	−33	+33	urban, SW [*Pandithurai et al.*, 2004]
Central India	Feb	+0.7 to −11	−15 to −40		urban and rural, SW [*Ganguly et al.*, 2005c]
AS	Mar–Apr	−12	−27	+15	polluted marine, SW [*Moorthy et al.*, 2005a]
AS	Nov–Mar	−6.1 to −3.8	−5.5 to −16.2	+15	SW + LW [*Satheesh et al.*, 2006]
BOB	Mar	−4	−27	+23	polluted marine, SW [*Satheesh*, 2002a]
BOB	Feb	−10.6	−26.6	+16	SW [*Ganguly et al.*, 2005a]
IO	Feb–Mar	−10	−29	+19	polluted marine, SW [*Satheesh et al.*, 2002]

[a]Unit is W m^{-2}. "AS," "BOB" and "IO" represent Arabian Sea, Bay of Bengal and Indian Ocean, respectively.

using our model for the GB. At this condition, the TOA and surface forcing efficiency in the SW calculated from the model are −89 and −24 W m^{-2} (per unit optical depth). For LW forcing, as it is not much sensitive to RH, we have considered the same efficiency values estimated for Kanpur. *Ramanathan and Ramana* [2005] have calculated the dry season (October–May) average surface forcing for the GB considering an average surface forcing efficiency value of −73 W m^{-2}, which is very close to our model-estimated value at Kanpur. Their value is averaged for the winter, spring and summer seasons, while it is obvious that with increase in surface albedo during the summer, the surface forcing will increase. Also, they have considered the surface and TOA forcing efficiency values of Kathmandu (a station in the Himalayan mountain range) to be valid for the GB.

[42] We considered MODIS-derived $AOD_{0.55}$ data, which show a mean value of 0.36 ± 0.14 during the winter season (December 2004 to February 2005). The TOA and surface forcings were obtained by multiplying the corresponding efficiency values in SW and LW. Thus the mean TOA and surface forcing for the GB during the winter season come out to be −8.6 and −32 W m^{-2} in SW and +2.2 and +1.8 W m^{-2} in the LW. In comparison, *Ramanathan and Ramana* [2005] obtained SW TOA and surface forcing values of zero and −32 ± 6 W m^{-2}. This is not surprising, as in the summer, the combined effect of drier atmosphere and enhanced surface albedo in the GB changes the TOA forcing from negative to zero, even becomes positive during the dust events [*Chinnam et al.*, 2006]. In the summer, during the dust events in May, SW TOA forcing in Kanpur was estimated to be +11 ± 0.7 W m^{-2} [*Chinnam et al.*, 2006], which clearly indicates that if the forcing is averaged for the dry season (i.e., October–May), TOA forcing would shift toward zero or even positive. Recently, *Sarkar et al.* [2006] have used CERES earth radiation budget data for estimation of TOA forcing over India. They have found that TOA forcing during the winter season over the major cities in the GB varies from −4.5 to −18 W m^{-2}. The TOA and surface forcings over the major cities (shown in Figure 1) in the GB, other populated cities in India and the adjacent oceans are listed in Table 5 for comparative study. It can be commented that our estimates of TOA forcing lie within the range given by *Sarkar et al.* [2006].

[43] All the major cities in the GB have similar kind of atmospheric forcing values (> +30 W m^{-2}), implying that the effect of pollution is maximum over the central GB (covering these cities, Figure 1) during the winter. *Pant et al.* [2006] have studied the aerosol optical properties and estimated the radiative forcing during the same period at a high-altitude location, Nainital in the foothills of Himalayas, which provides the background to compare the results from polluted regions in the GB. The atmospheric forcing in those populated urban areas is 7–9 times higher than that over Nainital. Comparison with the wintertime forcing values over the adjacent oceans reveals that the atmospheric forcing in the GB (+23.8 W m^{-2}) is higher than atmospheric forcing over the oceans. The average F_S over GB (∼3.7 for SW) is 23% higher than $F_S$over the Indian Ocean, implying higher concentration of absorbing aerosols in the GB. The net atmospheric forcing in the GB translates into a heating rate of 0.67 K day^{-1} for the lower atmosphere. The aerosols over the GB reduce the solar radiation reaching the surface by ∼19%, which is significant in terms of their effect on the boundary layer stability and humidity profile [*Ramanathan and Ramana*, 2005]. Our model, based on direct simultaneous measurements of size-segregated aerosol composition and physical parameters, can be very helpful in improvement of the current understanding of these issues along with the effect of the aerosols on long-term climate changes over the GB, which is the most populated and probably the most polluted river basin in the world.

9. Summary and Conclusions

[44] An aerosol model, representative of the GB for the winter season was developed from the collocated aerosol physical, chemical and optical measurements. The major conclusions of our study are as follows:

[45] 1. Mean $AOD_{0.55,}$ over the entire GB, is high (0.36 ± 0.14) during the winter season compared to that over the southern and central India. The observed aerosol optical properties over the GB are dominated by the anthropogenic

aerosols, whose relative contribution to the total extinction has been estimated maximum to be 83%.

[46] 2. $(NH_4)_2SO_4$ is the most dominant species, which contributes ~30% to the $AOD_{0.5}$,followed by NO_3^- (~24%), salt (~18%), dust (~17%) and BC (~11%). It should be mentioned here that the organics were not measured. The relative contribution of $(NH_4)_2SO_4$, NO_3^- and salt decrease with wavelength and that of dust increases three times, whereas, relative share of BC is spectrally constant.

[47] 3. The scattering coefficient in the fine mode fraction strongly depends on the RH, where, it shows a sharp rise after 80% RH. As, 88% extinction is due to the fine mode scattering, the observed composite aerosol optical properties are strongly influenced by RH. The spectral variation of the absorption coefficient suggests that the major source for the BC in this region is fossil fuel.

[48] 4. A parameterized equation was developed, which reproduces the observed AOD up to 76% (with RMS error of 0.134) by the surface concentration of the chemical species.

[49] 5. The spectral variation of ω_0 in the coarse mode suggests mixing of BC and dust in the GB. Although the model-derived AOD spectrum is steeper than AERONET-retrieved AOD spectrum, the SSA and g in close agreement implies that the model is able to reproduce the aerosol radiative properties quite well.

[50] 6. The mean clear-sky and diurnally averaged TOA and the surface radiative forcing at the SW for the composite aerosol model over Kanpur are -13 ± 3 and -43 ± 8 W m^{-2}, respectively. The corresponding longwave forcings are 3.6 ± 0.7 and 2.9 ± 0.6 W m^{-2}. Extending our model over the GB, the net mean TOA and surface forcing come out to be -6.4 and -30.2 W m^{-2} with an overall uncertainty of 15%. High atmospheric absorption (+23.8 W m^{-2}) over the entire GB transforms into a heating rate of 0.67 K day^{-1}, which is 25% higher than the INDOEX values.

[51] **Acknowledgments.** This work is carried out under the research project sponsored by DST-ICRP program. We appreciate the efforts of PIs in establishing and maintaining the Kanpur AERONET and Solar Radiation Network site. We acknowledge two reviewers for giving valuable comments which helped us in improving the original version of the manuscript.

References

Babu, S. S., and K. K. Moorthy (2002), Aerosol black carbon over a tropical station in India, *Geophys. Res. Lett.*, *29*(23), 2098, doi:10.1029/2002GL015662.

Babu, S. S., S. K. Satheesh, and K. K. Moorthy (2002), Aerosol radiative forcing due to enhanced black carbon at an urban site in India, *Geophys. Res. Lett.*, *29*(18), 1880, doi:10.1029/2002GL015826.

Bergstrom, R. W., P. Pilewskie, J. Pommier, M. Rabbette, P. B. Russell, B. Schmid, J. Redemann, A. Higurashi, T. Nakajima, and P. K. Quinn (2004), Spectral absorption of solar radiation by aerosols during ACE-Asia, *J. Geophys. Res.*, *109*, D19S15, doi:10.1029/2003JD004467.

Bond, T. C. (2001), Spectral dependence of visible light absorption by carbonaceous particles emitted from coal combustion, *Geophys. Res. Lett.*, *28*(21), 4075–4078.

Chandra, S., S. K. Satheesh, and J. Srinivasan (2004), Can the state of mixing of black carbon aerosols explain the mystery of 'excess' atmospheric absorption?, *Geophys. Res. Lett.*, *31*, L19109, doi:10.1029/2004GL020662.

Chate, D. M., and T. S. Pranesha (2004), Field measurements of submicron aerosol concentration during cold season in India, *Curr. Sci.*, *86*(12), 1610–1613.

Chinnam, N., S. Dey, S. N. Tripathi, and M. Sharma (2006), Dust events in Kanpur, northern India: Chemical evidence for source and implications to radiative forcing, *Geophys. Res. Lett.*, *33*, L08803, doi:10.1029/2005GL025278.

Clarke, A. D., et al. (2004), Size distributions and mixtures of dust and black carbon aerosols in Asian outflow: Physiochemistry and optical properties, *J. Geophys. Res.*, *109*, D15S09, doi:10.1029/2003JD004378.

Dey, S., S. N. Tripathi, R. P. Singh, and B. N. Holben (2004), Influence of dust storms on aerosol optical properties over the Indo-Gangetic basin, *J. Geophys. Res.*, *109*, D20211, doi:10.1029/2004JD004924.

Dey, S., S. N. Tripathi, R. P. Singh, and B. N. Holben (2005), Seasonal variability of aerosol parameters over Kanpur, an urban site in Indo-Gangetic basin, *Adv. Space Res.*, *36*, 778–782.

Dubovik, O., and M. D. King (2000), A flexible inversion algorithm for retrieval of aerosol optical properties from Sun and sky radiance measurements, *J. Geophys. Res.*, *105*(D16), 20,673–20,696.

Dubovik, O., B. N. Holben, T. F. Eck, A. Smirnov, Y. J. Kaufman, M. D. King, D. Tanre, and I. Slutsker (2002), Variability of absorption and optical properties of key aerosol types observed in worldwide locations, *J. Atmos. Sci.*, *59*, 590–608.

Ganguly, D., A. Jayaraman, and H. Gadhavi (2005a), In situ ship cruise measurements of mass concentration and size distribution of aerosols over Bay of Bengal and their radiative impacts, *J. Geophys. Res.*, *110*, D06205, doi:10.1029/2004JD005325.

Ganguly, D., A. Jayaraman, H. Gadhavi, and T. Rajesh (2005b), Features in wavelength dependence of aerosol absorption observed over central India, *Geophys. Res. Lett.*, *32*, L13821, doi:10.1029/2005GL023023.

Ganguly, D., H. Gadhavi, A. Jayaraman, T. A. Rajesh, and A. Misra (2005c), Single scattering albedo of aerosols over central India: Implications for the regional aerosol radiative forcing, *Geophys. Res. Lett.*, *32*, L18803, doi:10.1029/2005GL023903.

Garland, R. M., M. E. Wise, M. R. Beaver, H. L. DeWitt, A. C. Aiken, J. L. Jimenez, and M. A. Tolbert (2005), Impact of palmitic acid coating on water uptake and loss of ammonium sulfate particles, *Atmos. Chem. Phys.*, *5*, 1951–1961.

Girolamo, L. D., et al. (2004), Analysis of Multi-angle Imaging Spectro-Radiometer (MISR) aerosol optical depths over greater India during winter 2001–2004, *Geophys. Res. Lett.*, *31*, L23115, doi:10.1029/2004GL021273.

Hess, M., P. Koepke, and I. Schultz (1998), Optical properties of aerosols and clouds: The software package OPAC, *Bull. Am. Meteorol. Soc.*, *79*, 831–844.

Hignett, P., J. P. Taylor, P. N. Francis, and M. D. Glew (1999), Comparison of observed and modeled direct aerosol forcing during TARFOX, *J. Geophys. Res.*, *104*, 2279–2287.

Holben, B. N., et al. (2001), An emerging ground-based aerosol climatology: Aerosol optical depth from AERONET, *J. Geophys. Res.*, *106*, D11, 12,067–12,097.

Houghton, J. T., Y. Ding, D. J. Griggs, M. Noguer, P. J. van der Winden, and X. Dai (Eds.) (2001), *Climate Change 2001: The Scientific Basis. Contribution of Working Group 1 to the Third Assessment Report*, 881 pp., Cambridge Univ. Press, New York.

Jacobson, M. Z. (2000), A physically-based treatment of elemental carbon optics: Implications for global direct forcing of aerosols, *Geophys. Res. Lett.*, *27*(2), 217–220.

Jethva, H., S. K. Satheesh, and J. Srinivasan (2005), Seasonal variability of aerosols over the Indo-Gangetic basin, *J. Geophys. Res.*, *110*, D21204, doi:10.1029/2005JD005938.

Kirchstetter, T. W., T. Novakov, and P. V. Hobbs (2004), Evidence that the spectral dependence of light absorption by aerosols is affected by organic carbon, *J. Geophys. Res.*, *109*, D21208, doi:10.1029/2004JD004999.

Kotchenruther, R. A., P. V. Hobbs, and D. A. Hegg (1999), Humidification factors for atmospheric aerosols off the mid-Atlantic coast of the United States, *J. Geophys. Res.*, *104*(D2), 2239–2251.

Liou, K. N. (2002), *An Introduction to Atmospheric Radiation*, 583 pp., Elsevier, New York.

Mallet, M., J. C. Rogers, S. Despiau, J. P. Putaud, and O. Dubovik (2004), A study of the mixing state of black carbon in urban zone, *J. Geophys. Res.*, *109*, D04202, doi:10.1029/2003JD003940.

Malm, W. C., J. F. Sisler, D. Huffman, R. A. Eldred, and T. A. Cahill (1994), Spatial and seasonal trends in particle concentration and optical extinction in United States, *J. Geophys. Res.*, *99*(D1), 1347–1370.

Moorthy, K. K., S. S. Babu, and S. K. Satheesh (2003), Aerosol spectral depths over the Bay of Bengal: Role of transport, *Geophys. Res. Lett.*, *30*(5), 1249, doi:10.1029/2002GL016520.

Moorthy, K. K., S. S. Babu, and S. K. Satheesh (2005a), Aerosol characteristics and radiative impacts over the Arabian Sea during the intermonsoon season: Results from ARMEX Field Campaign, *J. Atmos. Sci.*, *62*, 192–206.

Moorthy, K. K., et al. (2005b), Wintertime spatial characteristics of boundary layer aerosols over peninsular India, *J. Geophys. Res.*, *110*, D08207, doi:10.1029/2004JD005520.

Pandithurai, G., R. T. Pinker, T. Takamura, and P. C. S. Devara (2004), Aerosol radiative forcing over a tropical urban site in India, *Geophys. Res. Lett.*, *31*, L12107, doi:10.1029/2004GL019702.

Pant, P., P. Hegde, U. C. Dumka, R. Sagar, S. K. Satheesh, K. K. Moorthy, A. Saha, and M. K. Srivastava (2006), Aerosol characteristics at a high-altitude location in central Himalayas: Optical properties and radiative forcing, *J. Geophys. Res.*, *111*, D17206, doi:10.1029/2005JD006768.

Parmar, R. S., G. S. Satsangi, M. Kumari, A. Lakhani, S. S. Srivastava, and S. Prakash (2001), Study of size distribution of atmospheric aerosol at Agra, *Atmos. Environ.*, *35*, 693–702.

Pierluissi, J. H., and G.-S. Peng (1985), New molecular transmission band models for LOWTRAN, *Opt. Eng.*, *24*(3), 541–547.

Pilnis, C., S. N. Pandis, and J. H. Seinfeld (1995), Sensitivity of direct climate forcing of atmospheric aerosols to aerosol size and composition, *J. Geophys. Res.*, *100*(D9), 18,739–18,754.

Podgorny, I. A., W. C. Conant, V. Ramanathan, and S. K. Satheesh (2000), Aerosol modulation of atmospheric and surface solar heating rates over the tropical Indian Ocean, *Tellus, Ser. B*, *52*, 947–958.

Ramachandran, S. (2005a), Premonsoon shortwave aerosol radiative forcings over the Arabian Sea and tropical Indian Ocean: Yearly and monthly mean variabilities, *J. Geophys. Res.*, *110*, D07207, doi:10.1029/2004JD005563.

Ramachandran, S. (2005b), Aerosol radiative forcing over Bay of Bengal and Chennai: Comparison with maritime, continental, and urban aerosol models, *J. Geophys. Res.*, *110*, D21206, doi:10.1029/2005JD005861.

Ramanathan, V., and M. V. Ramana (2005), Persistent, widespread, and strongly absorbing haze over the Himalayan foothills and the Indo-Ganges plains, *Pure Appl. Geophys.*, *162*, 1609–1626.

Ramanathan, V., et al. (2001), Indian Ocean Experiment: An integrated analysis of the climate forcing and effects of the great Indo-Asian haze, *J. Geophys. Res.*, *106*, 28,371–28,398.

Reddy, M. S., and C. Venkataraman (2000), Atmospheric optical and radiative effects of anthropogenic aerosols constituents from India, *Atmos. Environ.*, *34*, 4511–4523.

Reddy, M. S., and C. Venkataraman (2002a), Inventory of aerosol and sulphur dioxide emissions from India: I-Fossil fuel combustion, *Atmos. Environ.*, *36*, 677–697.

Reddy, M. S., and C. Venkataraman (2002b), Inventory of aerosol and sulphur dioxide emissions from India: II-Biomass combustion, *Atmos. Environ.*, *36*, 699–712.

Ricchiazzi, P., S. Yang, C. Gautier, and D. Sowle (1998), SBDART: A research and teaching software tool for plane-parallel radiative transfer in the earth's atmosphere, *Bull. Am. Meteorol. Soc.*, *79*, 2101–2114.

Sarkar, S., R. Chokngamwong, G. Cervone, R. P. Singh, and M. Kafatos (2006), Variability of aerosol optical depth and aerosol forcing over India, *Adv. Space Res.*, *37*(12), 2153–2159.

Satheesh, S. K. (2002a), Radiative forcing by aerosols over Bay of Bengal region, *Geophys. Res. Lett.*, *29*(22), 2083, doi:10.1029/2002GL015334.

Satheesh, S. K. (2002b), Aerosol forcing over land: Effect of surface and cloud reflection, *Ann. Geophys.*, *20*, 2105–2109.

Satheesh, S. K., and V. Ramanathan (2000), Large differences in tropical aerosol forcing at the top of the atmosphere and Earth's surface, *Nature*, *405*, 60–63.

Satheesh, S. K., V. Ramanathan, X. L-Jones, J. M. Lobert, I. A. Podgorny, J. M. Prospero, B. N. Holben, and N. G. Loeb (1999), A model for the natural and anthropogenic aerosols over the tropical Indian Ocean derived from Indian Ocean Experiment data, *J. Geophys. Res., 104*, D22, 27,421–27,440.

Satheesh, S. K., V. Ramanathan, B. N. Holben, K. K. Moorthy, N. G. Loeb, H. Maring, J. M. Prospero, and D. Savoie (2002), Chemical, microphysical, and radiative effects of Indian Ocean aerosols, *J. Geophys. Res.*, *107*(D23), 4725, doi:10.1029/2002JD002463.

Satheesh, S. K., K. K. Moorthy, Y. J. Kaufman, and T. Takemura (2006), Aerosol optical depth, physical properties and the radiative forcing over the Arabian Sea, *Meteorol. Atmos. Phys.*, *91*, 45–62.

Schnaiter, M., H. Hovath, O. Mohler, K. H. Naumann, H. Saathoff, and O. W. Schock (2003), UV-VIS-NIR spectral optical properties of soot and soot-containing aerosols, *J. Aerosol Sci.*, *34*, 1421–1444.

Singh, R. P., S. Dey, S. N. Tripathi, V. Tare, and B. N. Holben (2004), Variability of aerosol parameters over Kanpur, northern India, *J. Geophys. Res.*, *109*, D23206, doi:10.1029/2004JD004966.

Sokolik, I. N., and O. B. Toon (1999), Incorporation of mineralogical composition into models of the radiative properties of the mineral aerosol from UV to IR wavelength, *J. Geophys. Res.*, *104*(D8), 9423–9444.

Stamnes, K., S. Tsay, W. Wiscombe, and K. Jayaweera (1988), Numerically stable algorithm for discrete-ordinate-method radiative transfer in multiple scattering and emitting layered media, *Appl. Opt.*, *27*, 2502–2509.

Strahler, A. H., et al. (1999), MODIS BRDF/Albedo Product: Algorithm Theoretical Basis Document Version 5.0. (Available at http://modis.gsfc.nasa.gov/data/atbd/land_atbd.php)

Sumanth, E., K. Mallikarjuna, J. Stephen, M. Moole, V. Vinoj, S. K. Satheesh, and K. K. Moorthy (2004), Measurements of aerosol optical depths and black carbon over Bay of Bengal during post-monsoon season, *Geophys. Res. Lett.*, *31*, L16115, doi:10.1029/2004GL020681.

Tare, V., et al. (2006), Measurements of atmospheric parameters during Indian Space Research Organization Geosphere Biosphere Program Land Campaign II at a typical location in the Ganga Basin: 2. Chemical properties, *J. Geophys. Res.*, *111*, D23210, doi:10.1029/2006JD007279.

Tripathi, S. N., S. Dey, A. Chandel, S. Srivastava, R. P. Singh, and B. N. Holben (2005a), Comparison of MODIS and AERONET derived aerosol optical depth over the Ganga Basin, India, *Ann. Geophys.*, *23*, 1093–1101.

Tripathi, S. N., S. Dey, V. Tare, S. K. Satheesh, S. Lal, and S. Venkataramani (2005b), Enhanced layer of black carbon in a north Indian industrial city, *Geophys. Res. Lett.*, *32*, L12802, doi:10.1029/2005GL022564.

Tripathi, S. N., S. Dey, V. Tare, and S. K. Satheesh (2005c), Aerosol black carbon radiative forcing at an industrial city in northern India, *Geophys. Res. Lett.*, *32*, L08802, doi:10.1029/2005GL022515.

Tripathi, S. N., et al. (2006), Measurements of atmospheric parameters during Indian Space Research Organization Geosphere Biosphere Programme Land Campaign II at a typical location in the Ganga basin: 1. Physical and optical properties, *J. Geophys. Res.*, *111*, D23209, doi:10.1029/2006JD007278.

Vinoj, V., S. S. Babu, S. K. Satheesh, K. K. Moorthy, and Y. J. Kaufman (2004), Radiative forcing by aerosols over the Bay of Bengal region derived from ship borne, island-based, and satellite (Moderate-Resolution Imaging Spectroradiometer) observations, *J. Geophys. Res.*, *109*, D05203, doi:10.1029/2003JD004329.

Whitby, K. T. (1978), The physical characteristics of sulfur aerosols, *Atmos. Environ.*, *12*, 135–159.

S. Dey and S. N. Tripathi, Department of Civil Engineering, Indian Institute of Technology, Kanpur 208016, India. (snt@iitk.ac.in)